Acid−Base Characterization of Aluminum Oxide Surfaces with XPS

J. van den Brand,*,† P. C. Snijders,‡ W. G. Sloof,§ H. Terryn,† and J. H. W. de Wit†,§

Netherlands Institute for Metals Research, Rotterdamseweg 137, 2628 AL Delft, The Netherlands, Kavli Institute of NanoScience Delft, Delft University of Technology, Lorentzweg 1, 2628 CJ Delft, The Netherlands, and Department of Materials Science and Engineering, Delft University of Technology, Rotterdamseweg 137, 2628 AL, Delft, The Netherlands

Received: December 16, 2003; In Final Form: March 8, 2004

The localized acid−base properties of different, aluminum oxide thin layer surfaces have been evaluated with X-ray photoelectron spectroscopy (XPS). Five types of oxide layers were studied, which were produced by oxidizing aluminum in a vacuum, with an alkaline and acidic pretreatment, and in boiling water. The photoelectron core level binding energies, as measured with XPS, are evaluated for this purpose, while taking into consideration the initial and final state effects. For the structurally comparable oxides, the shifts in the O 1s binding energies are determined by their initial state chemistry. The values of the O 1s binding energy can be directly related to the surface-averaged charge on the O anions. For the Al cations, a correlation between the photoelectron core level binding energy shift and changes in the initial state chemistry was observed, but the Al 2p binding energy shifts were found to be partially due to changes in extra-atomic relaxation. The measured Al 2p binding energies and the binding energies of the resolved OH and O components in the O 1s peak showed that the studied aluminum oxides have OH sites with the same Brönsted/Lewis acid−base properties, O sites with the same Lewis base properties, and Al sites with very similar Lewis acid properties. The pseudoboehmite oxide, obtained by boiling aluminum in water, exhibits more basic O, OH, and Al sites. This oxide deviates structurally from the other oxides studied, resulting in a lower extra-atomic relaxation and Madelung potential contribution to the binding energies.

I. Introduction

The acid−base properties of an oxide surface play a major role in interfacial reactions and are therefore important in fields such as catalysis, adhesion, corrosion, and wetting.[1−4] This macroscopic property is on the atomic scale determined by a large number of different reactive sites, which each have their own acid−base properties. The oxide surface can be considered to consist of three different types of sites. The O anions can act as electron-donating Lewis base sites and incompletely coordinated cations as electron-accepting Lewis acid sites, and the OH anion can act as either a Lewis acid or base, but also as a proton-exchanging Brönsted acid−base site.[4] For a localized description of the acid−base events that can occur on the oxide surface, an understanding of the acid−base properties of these separate sites is required. The X-ray photoelectron spectroscopy (XPS) analysis technique enables the study of these acid−base properties. It probes the electronic structure of a material and specifically enables one to distinguish separate sites related to the elemental constituents. XPS is widely used to determine the valence state of ions,[5] the nature of bonding (e.g., ionicity/covalency),[6−8] and acid−base properties of oxides.[3,9−10]

In this work, the localized acid−base properties of a set of five different, amorphous aluminum oxide thin layers are investigated with XPS. These layers represent typical layers that can develop on aluminum surfaces and are frequently encountered in fields such as adhesion and lithographic plating[11−13] and as models to investigate alumina-based catalysts.[14] The oxide layers studied were produced by oxidizing aluminum in a vacuum, with an alkaline and acidic pretreatment, and in boiling water. To evaluate the localized acid−base properties of their Al, O, and OH sites, the Al 2p and O 1s electron core-level binding energies are evaluated, while taking into consideration the initial and final state effects in the photoelectron emission process, and the O 1s peak is resolved into its OH and O components. To study the oxide layer and chemistry at the surface and the interior of the layers, angle-resolved XPS was performed. To our knowledge, such a detailed analysis of the correctness of the use of binding energies for evaluating the acid−base properties of the Al, O, and OH sites has not been performed before.

II. Interpretation of XPS Core Level Binding Energies

According to the simple electrostatic potential model introduced by Siegbahn et al.,[15] the binding energy shift $\Delta E_B(A)$, observed for the core level of an atom A in two different materials can be described with the following equation:[5,15,16]

$$\Delta E_B(A) = k\Delta q + \Delta V_M - \Delta R^{ea} \quad (1)$$

In this equation, Δq is the change in effective electronic charge on the A atom with k being a constant. The ΔV_M term is the change in the Madelung potential, which describes the electrostatic interaction between the single atom A and charges on the other atoms grouped in the lattice around A. The term

* To whom correspondence should be addressed. E-mail: j.vandenbrand@tnw.tudelft.nl.
† Netherlands Institute for Metals Research.
‡ Kavli Institute of NanoScience Delft, Delft University of Technology.
§ Department of Materials Science and Engineering, Delft University of Technology.

10.1021/jp037877f CCC: $27.50 © 2004 American Chemical Society
Published on Web 04/21/2004

ΔR^{ea} arises from the extra-atomic charge rearrangement or relaxation that occurs in response to the core hole created in the photoelectron process. Equation 1 can be divided into two parts. The first part ($k\Delta q + \Delta V_M$) represents the *initial state* chemistry of the photoionized atoms/ions and is the important parameter for the localized acid−base properties considered here. The second part, ΔR^{ea}, represents the *final state* contribution to the binding energy due to the photoionization process in the measuring technique. The final state and Madelung potential contributions to the binding energies are often neglected and k is assumed to be constant in the XPS analysis of oxides.[5,9] A direct relation between the change in electronic charge on the ions or atoms and measured binding energy shift is then obtained, i.e., $\Delta E_B(A) = k\Delta q$. For a cation ($q > 0$) a more positive charge will then result in an higher binding energy, while for an anion ($q < 0$), a more negative charge will result in a lower binding energy. This approach often leads to correct results,[17,18] but in some cases it was found that either the Madelung potential or extra-atomic relaxation showed a dominant contribution to the binding energy shifts.[16,19,20]

By using the Auger parameter concept introduced by Wagner,[21] the contribution of the final state effects to the binding energy can be evaluated. The Auger parameter is defined as $\alpha' = E_k(C'C''C''') + E_B(C)$,[16,22] with $E_k(C'C''C''')$ being the kinetic energy of an Auger transition involving the C′, C″, and C‴ core electron levels. For a shift in this Auger parameter $\Delta\alpha'$:[23]

$$\Delta\alpha' = 2\Delta R^{ea} \tag{2}$$

which can therefore be used to evaluate the effect of changes in extra-atomic relaxation. The Auger parameter is insensitive to charging effects and Fermi level changes because the effects cancel out in the calculation.[16] The Auger parameter is considered to be a sensitive indicator to study changes in the local environment of the core ionized atom.[22,24−27] In addition to the Auger parameter, also a parameter can be derived that corresponds to the initial state part of the binding energy (cf. eq 1). This initial state parameter, denoted as β, is defined as $[E_k(C'C''C'') + 3E_B(C)]$ and a shift in this parameter corresponds to[16]

$$\Delta\beta = 2\Delta[V_M + kq] \tag{3}$$

and can therefore be used to evaluate the effect of changes in the initial state chemistry. In contrast with the Auger parameter, this initial state parameter is sensitive to errors in charging corrections and work function changes and an error in one of these will result in a twice as large error in the calculated values. The Madelung potential contribution to the initial state parameter can be calculated if detailed structural knowledge of the atomic arrangement of the considered oxide is available.[10,16,20,24] A direct separation of the contributing terms to the initial state parameter is then possible. For most amorphous aluminum oxides—as studied in this work—such detailed structural information is not available. However, an alternative approach can be followed that allows a direct evaluation of the electronic charge q on the O anion in the oxide. Using an electrostatic model, Ascarelli et al.[28] demonstrated that the Auger peak separation $E_k(O\ KL_{23}L_{23}) - E_k(O\ KL_1L_{23})$ is a direct measure of this electronic charge, independent of Madelung potential and relaxation effects. An increase in this peak separation indicates an increasing electronic charge on the O anion. For a large set of different aluminum oxides it was found that this peak distance indeed correctly described trends in ionicities.[29] Similar approaches were followed by others.[30,31] Since the Fermi level is used as a reference for the energy of the emitted photoelectrons in XPS, a change of the Fermi level will cause a homogeneous binding energy shift of the core electron peaks.[5,32,33] This Fermi-level shift is not included in eq 1. Such a Fermi-level shift can be caused by impurities, defects, or a nonstoichiometric composition in nonconductive materials, which all introduce states in the band gap.

III. Experimental Details and Data Evaluation

Oxide Layers. In this work, a set of five different types of aluminum oxide layers were investigated. All oxide layers were studied as freshly prepared and the time between preparation and introduction into the XPS apparatus was no more than 10 min.

Anhydrous, Amorphous Aluminum Oxide. A disc-shaped specimen with a diameter of 10 mm and a thickness of 1 mm of recrystallized aluminum (>99.99 wt % purity) was used. First, the surface of the sample was polished in several subsequent steps. The final polishing step was done with a neutral polishing slurry with 0.025 μm aluminum oxide particles (Struers). Then, the sample was chemically polished for 1.5 min in a solution consisting of 70 mL of H_3PO_4, 25 mL of H_2SO_4, and 5 mL of HNO_3 at a temperature of 85 °C. Finally, the samples were rinsed with deionized water and blown dry with compressed nitrogen. The sample was subsequently mounted in the UHV preparation chamber (base pressure $< 2 \times 10^{-8}$ Pa) that was directly coupled to the XPS instrument. First, the native oxide layer was sputtered away with a focused Ar^+ beam. Next, the sample and sample holder were outgassed by repeated annealing for 4 h at 773 K and subsequent cleaning with a focused Ar^+ beam scanning the specimen surface area at room temperature. The procedure is discussed elsewhere in more detail.[34,35] As a final step, the sample was oxidized by admitting pure oxygen (99.9998 vol %) at room temperature to a pressure of 1.33×10^{-4} Pa for 1 h. Next, the sample was transferred into the XPS system for analysis without exposure to the ambient.

Evaporated and Oxidized Aluminum. First, an approximately 100 nm thick aluminum layer was deposited onto a cleaned $12 \times 12 \times 1$ mm^3 glass slide (Agar Scientific) by evaporation of 99.998 wt % pure aluminum at a base pressure of 3×10^{-5} Pa, using a vacuum evaporation unit (Balzers BAE 250). Pure oxygen (99.998 vol %) was subsequently admitted to a pressure of about 1×10^{-2} Pa for 1 h and finally the vacuum chamber was filled with pure oxygen to ambient pressure.

Acid-Pretreated Aluminum. For this and the subsequent oxide types, an AA1050 aluminum alloy was used (99.5 wt % of Al, 0.04 wt % of Fe, and 0.25 wt % of Si). First, the surface of the sample ($12 \times 12 \times 1$ mm^3) was polished in several subsequent steps. The final polishing step was done with a neutral polishing slurry with 0.025 μm aluminum oxide particles (Struers). The samples were cleaned in hot chloroform (99+ vol % pure). Thereafter, the substrates were immersed in a 30 vol % HNO_3 solution (chemically pure) in deionized water for 30 s. Finally, the substrates were thoroughly rinsed for at least 3 min with deionized water and blown dry with compressed clean air.

Alkaline-Pretreated Aluminum. After being polished and cleaned, the samples were mildly etched in a pH 12.5 solution made with NaOH (97+ vol % pure) in deionized water for a period of 30 s. The substrates were then thoroughly rinsed for at least 3 min with deionized water and blown dry with compressed clean air.

Pseudoboehmite Oxide. After being polished and cleaned, the samples were immersed in boiling deionized water for a period of 60 s, which results in the formation of a thick pseudoboehmite

TABLE 1: Measured O 1s and Al 2p Core Level Binding Energies and O $KL_{23}L_{23}$ and Al $KL_{23}L_{23}$ Kinetic Energies of the Various Aluminum Oxides

type of oxide layer	angle (deg)	O 1s BE (fwhm) (eV)	Al 2p BE (fwhm) (eV)	E(Al−O) (eV)	O $KL_{23}L_{23}$ KE (eV)	Al $KL_{23}L_{23}$ KE (eV)
anhydrous amorphous oxide	45	531.0 (2.2)	74.3 (2.1)	456.7	509.0 (6.5)	1387.6 (2.2)
evaporated and oxidized	45	531.2 (2.3)	74.4 (1.8)	456.8	508.5 (6.8)	1387.6 (2.1)
	15	531.1 (2.5)	74.3 (1.8)	456.8	508.5 (7.0)	1387.6 (2.2)
acid pretreated	45	531.4 (2.5)	74.6 (1.9)	456.9	508.3 (6.9)	1387.2 (2.3)
	15	531.4 (2.9)	74.4 (1.9)	457.0	508.5 (8.0)	1387.3 (2.2)
alkaline pretreated	45	531.5 (2.9)	74.7 (1.9)	456.8	508.3 (7.4)	1386.9 (2.2)
	15	531.6 (3.1)	74.6 (1.9)	457.1	508.3 (8.4)	1387.0 (2.1)
pseudoboehmite (boiled)	45	531.2 (3.0)	73.9 (2.2)	457.3	508.0 (8.5)	1387.6 (2.6)
	15	531.2 (3.1)	73.9 (2.2)	457.3	507.9 (9.0)	1387.5 (2.6)
estimated error (±)		0.05	0.05	0.1	0.1	0.1

(AlOOH) layer.[13,36] The samples were then allowed to dry for a few minutes in an upright position.

IV. XPS Analysis and Data Evaluation

Experimental Details. XPS spectra of the Al 2p, O 1s, and C 1s, O KLL, and Al KLL photoelectron lines were recorded with a step size of 0.1 eV for all oxide samples, using a PHI 5400 ESCA instrument (base pressure $<1 \times 10^{-8}$ Pa) set at a constant analyzer pass energy of 35.75 eV, using unmonochromatized incident Mg X-ray radiation (Mg $K\alpha_{1,2} = 1253.6$ eV). The energy scale of the Spherical Capacitor Analyzer (SCA) spectrometer was calibrated according to the procedure described in ref 37. For most oxides, two samples were investigated and for each sample, measurements were performed at takeoff angles of 45° and 15° with respect to the surface to study possible changes in chemistry toward the surface region. The obtained spectra were corrected for the presence of X-ray satellites and also corrected for the electron kinetic energy dependent transmission of the spectrometer by multiplying each spectral intensity with its corresponding kinetic energy.[38] For all samples investigated, the XPS survey spectra showed Al, O, and C to be the main elements with other elements only appearing at trace levels. For the anhydrous, amorphous oxide no carbon signal was detected. To correct for sample charging, the spectra were shifted to set the C−C/C−H components of the C 1s core level peak at a binding energy of 284.8 eV.[5] Only for the anhydrous, amorphous oxide this was not possible due to the absence of a contamination overlayer and the same charging shift was applied as on the evaporated and oxidized aluminum. Both oxides show the same initial Al 2p metal−Al 2p oxide shift of 2.8 eV, and have a comparable thickness,[39] which demonstrates that these oxides are comparable.[40−42]

Data Evaluation. For the determination of the oxidic Al 2p core level binding energies and Al $KL_{23}L_{23}$ kinetic energies, the measured spectra were resolved into an oxidic and a metallic component in their respective binding energy regions. A procedure was used in which the metallic peak (obtained from a clean aluminum sample without an oxide layer) plus its associated Tougaard background and including the tail toward higher binding energies is reconstructed in the measured spectrum of the oxidized sample. This procedure is discussed elsewhere in detail.[43,44] For the O 1s, O KLL, and C 1s peaks, the binding energy positions were determined after subtraction of a simple Shirley-type background. Since the spectra only contain a small contribution of inelastically scattered electrons as compared to the intensity of the main peak, the result was found to be insensitive to the choice of type of background subtraction.[43] The various binding and kinetic energy positions were determined accurately by fitting of a third degree polynomial function through the top of the respective peaks. Curve-fitting of the O 1s photoelectron peak to determine the fraction of hydroxyls was performed in the 526−538 eV binding energy region, using a constrained fitting procedure in which the widths and shapes (mixed Gauss−Lorentz function) for the different fit components in the peak were allowed to change. However, the change was restricted to be the same for all components. The procedure is discussed in more detail in a previous work.[39] No restrictions were imposed on the binding energy positions of the components. In a previous investigation,[39] an analysis was performed of the layer thicknesses of the studied oxides. All thicknesses were found to be close to or much larger than 1 nm. For this reason, a contribution to the binding energies due to polarization of the underlying metal is not expected.[28] For both Al and O, Auger parameters α'_{Al} and α'_{O} have been calculated where α'_{Al} has been calculated as $[E_k(\text{Al } KL_{23}L_{23}) + E_B(\text{Al } 2p)]$ and α'_{O} as $[E_k(\text{O } KL_{23}L_{23}) + E_B(\text{O } 1s)]$. The initial state parameters β_{Al} and β_{O} have been respectively calculated as $[E_k(\text{Al } KL_{23}L_{23}) + 3E_B(\text{Al } 2p)]$ and $[E_k(\text{O } KL_{23}L_{23}) + 3E_B(\text{O } 1s)]$.

V. Results

Measured Core Level Binding Energies and Auger Kinetic Energies. The measured O 1s, Al 2p binding energies and O $KL_{23}L_{23}$, Al $KL_{23}L_{23}$ kinetic energies of the five different types of studied oxides at the two different takeoff angles are summarized in Table 1. The binding energy positions of both the O 1s and Al 2p peaks correspond well to values reported for comparable types of amorphous aluminum oxides.[45−50] A typical example of the Al KLL and O KLL Auger electron transition spectra is shown in Figure 1 with the associated peak designations. In Table 1 also the full-width at half-maxima (fwhm) of the O 1s and Al 2p peaks are listed. The different oxides clearly show variations in fwhm of the O 1s peak, but not in the Al 2p peak. The higher Al 2p peakwidth for the anhydrous amorphous oxide is due to a surface oxide component at a lower binding energy, as discussed in detail elsewhere.[26]

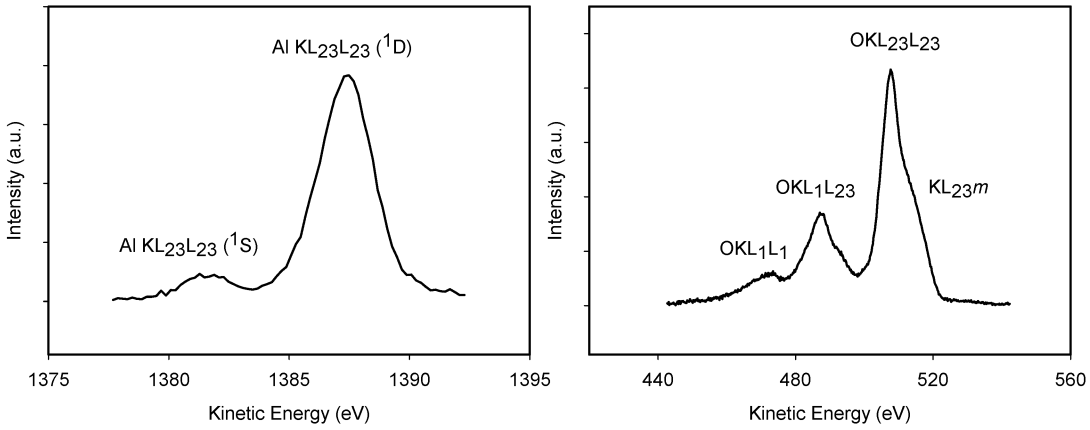

Figure 1. Al KLL and O KLL Auger electron spectra and designations for a pseudoboehmite oxide (Shirley-type background subtracted).

TABLE 2: Resolved Components in the O 1s Core Level Peak by Curve-Fitting of the Various Aluminum Oxides

type of oxide layer	angle (deg)	OH fraction (−)	O BE (eV)	OH BE (eV)
anhydrous amorphous oxide	45	0.00	530.9	−
evaporated and oxidized	45	0.11	531.0	532.4
	15	0.21	531.1	532.4
acid pretreated	45	0.25	531.1	532.4
	15	0.35	531.0	532.4
alkaline pretreated	45	0.30	531.0	532.4
	15	0.43	530.9	532.3
pseudoboehmite	45	0.49	530.5	532.0
(boiled)		0.01 H_2O		533.5
	15	0.47	530.4	531.8
		0.04 H_2O		533.7
estimated error (±)		0.05	0.05	0.05

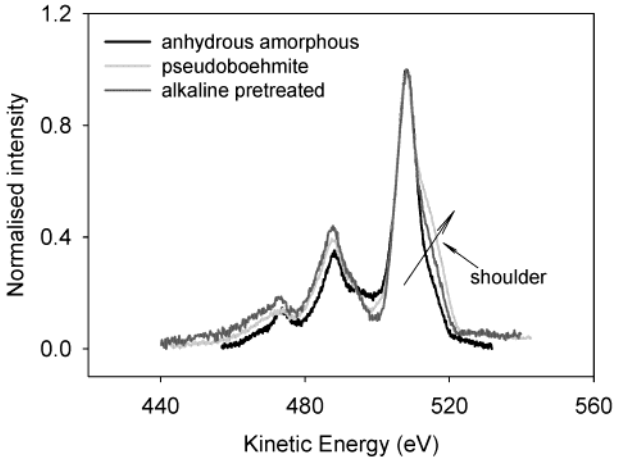

Figure 2. Measured O KLL spectra for anhydrous, alkaline-pretreated, and pseudoboehmite oxides after subtraction of a Shirley-type background. (Spectra are shifted to give the same O $KL_{23}L_{23}$ kinetic energy.)

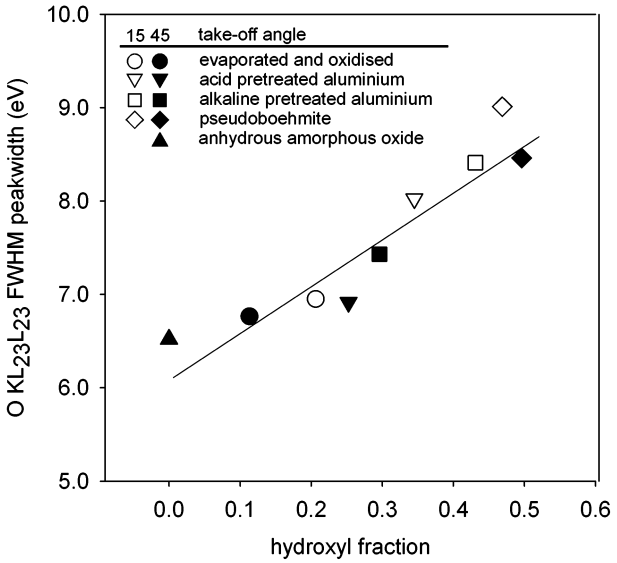

Figure 3. Full-width at half-maximum (fwhm) of O $KL_{23}L_{23}$ peak versus hydroxyl fraction as determined from curve fitting of the O 1s core level for the various aluminum oxides, at 15°and 45° takeoff angle.

For the pseudoboehmite oxide, the increase in Al 2p binding energy is likely due to charging effects. The increase in O 1s peakwidth can be ascribed entirely to the increase of the hydroxyl concentrations in the oxides, see ref 39. The different components constituting the O 1s peak, corresponding to O, OH and for pseudoboehmite also H_2O, were resolved by curve fitting. The values of the binding energies of these components and their relative fractions are reported in Table 2. These results are discussed in more detail in a previous work.[39]

It was observed that with changing hydroxyl concentration, the intensity of a shoulder on the high kinetic energy side of the O $KL_{23}L_{23}$ transition in the O KLL spectrum also changed. This is illustrated in Figure 2, where the O KLL spectra are shown for the anhydrous amorphous aluminum, alkaline-pretreated aluminum, and pseudoboehmite types of oxides. Such a shoulder is more often reported in the literature and has been ascribed to a $KL_{23}m$ transition,[51,52] in which a L_{23} hole on the central O anion is filled by an electron from a metal-like orbital. Other authors, however, associate this phenomenon with hydroxyls in an hydroxide,[53] or hydrogen bonding between different hydroxyls.[54] The shoulder has the effect of broadening of the O $KL_{23}L_{23}$ peak. In Figure 3, the O $KL_{23}L_{23}$ fwhm's are plotted versus the corresponding hydroxyl fractions. The relation between the O $KL_{23}L_{23}$ fwhm and the OH fraction was confirmed by an additional experiment in which a pseudoboehmite oxide was dehydrated in situ in a vacuum at a temperature of 300 °C. The *removal* of the hydroxyls from the oxide (as evidenced by a decreasing OH component in the O 1s core level peak) resulted in a significant *reduction* of the shoulder. As a clear correlation is observed between the hydroxyl fractions and the O $KL_{23}L_{23}$ peakwidth, the major part of this shoulder is not associated with a $KL_{23}m$ transition, but is related to the hydroxyls in the oxide layer.

Auger Parameters. The Auger parameters α'_O and α'_{Al} are considered to evaluate the contribution of the extra-atomic relaxation to the measured core level binding energies (cf. eq

TABLE 3: Al and O Auger Parameters for the Various Aluminum Oxides[a]

type of oxide layer	angle (deg)	α'_{Al} (eV)	α'_{O} (eV)
anhydrous amorphous oxide	45	1461.9	1039.9
evaporated and oxidized	45	1461.9	1039.7
	15	1461.9	1039.7
acid pretreated	45	1461.8	1039.7
	15	1461.7	1039.9
alkaline pretreated	45	1461.5	1039.7
	15	1461.4	1039.8
pseudoboehmite (boiled)	45	1461.5	1039.2
	15	1461.4	1039.1
estimated error (±)		0.1	0.1

[a] The corresponding core level binding energies are listed in Table 1.

2). The Auger parameters as determined for all oxides at both takeoff angles are summarized in Table 3. The various oxides exhibit an almost constant α'_O in the narrow 1039.7−1039.9 eV range. The pseudoboehmite oxide shows a significantly lower value of 1039.1−1039.2 eV. These α'_O values also do not change significantly when going from the bulk of the oxide layer (45° takeoff angle) to more toward the surface region (15° takeoff angle). The α'_O values must be considered as an average of the chemical environments of the OH and O ions in the oxide layers, because it was not possible to resolve the contribution of these constituents to the O KLL peak, see also ref 52. The α'_O values for the *amorphous* oxides studied here are not comparable to literature values given for *crystalline* oxides with a similar composition.[22] This is at least in part due to structural differences between the amorphous and crystalline oxides: a gradual transition from amorphous Al_2O_3 to crystalline γ-Al_2O_3 results in a gradual change in the α'_O from 1039.9 to 1038.9 eV.[27]

The α'_{Al} values of the studied oxides are in the range of 1461.4−1461.9 eV. These values also do not change significantly when going from the bulk toward the surface region of the oxide layer. The α'_{Al} value of pseudoboehmite (1461.5 eV) is lower than the value given by Wagner for crystalline boehmite (1461.8 eV)[22] and the values for the other oxides are higher than the value for crystalline γ-Al_2O_3 (1461.8 eV). The α'_{Al} values, however, do correspond well to structurally more comparable amorphous oxide layers. For anhydrous amorphous aluminum oxides, values of 1461.9 eV have recently been obtained[27,35] and about 0.4 eV lower values have been found for hydroxyl- containing oxide layers obtained by oxidation in H_2O/O_2 gas mixtures[51] and ambient-exposed native oxide layers, likely also containing hydroxyls.[55] It appears that there is a trend in which the α'_{Al} values decrease with an increase in hydroxyl concentration in the oxide layers. This can have the effect of lowering the α'_{Al} directly, due to the lower polarizability of the OH as compared to the O anion.[56] However, this conclusion does not appear to be fully justified. Upon removal of hydroxyls from a pseudoboehmite oxide through dehydroxylation by heating at 300 °C in a vacuum, see above, the Auger parameter did not show a significant increase again. Shifts of the α'_{Al} are often explained as changes in coordination number of the Al cations.[22] The presence of different coordination states is expected to show up as a broadening of the Al $KL_{23}L_{23}$ and Al 2p peaks.[10,17,57] Sometimes curve fitting of the Al $KL_{23}L_{23}$ peak or Al 2p peak is performed to distinguish states with a different coordination.[10,17,57] However, such an effect was not observed and all oxides showed an Al $KL_{23}L_{23}$ fwhm in the 2.1−2.3 eV range and the Al 2p peak in the 1.8−1.9 eV range, with only the pseudoboehmite oxide showing significantly higher values due to charging. The presence of different aluminum coordination states in the oxides can therefore be excluded as a possible explanation for the α'_{Al} shifts. The absence of different coordination states also suggests that the hydroxyls in the alkaline-pretreated, acid-pretreated, and evaporated and oxidized types of oxides are not present in separate $Al(OH)_3$ or AlOOH units in an "Al_2O_3 matrix"[49,58] but rather obtain isolated positions[50] as otherwise mixtures of different coordination states are expected to show up in the Al 2p and Al KLL peaks.

The much lower value of the α'_O for the pseudoboehmite oxide, see Table 3, indicates that the local environment around the O anion deviates significantly from that of the other oxides. In the crystalline boehmite, the Al cations reside in distorted octaedra of O ions. These octaedra are joined to form an interlocking double layer in which the oxygen anions are in a cubic-closed packing but the whole structure is not close-packed.[13,36] The double layers are linked by hydrogen bonds between hydroxyl ions in neighboring planes. As compared to the crystalline boehmite, the pseudoboehmite is structurally less well defined and further it has interlamellar water in its structure. As shown in ref 27, in the anhydrous amorphous oxide, the short-range ordering around the Al ions is the same as that in crystalline γ-Al_2O_3, i.e., both tetrahedrally and octahedrally coordinated Al ions exist in the same ratio as in the well-defined crystalline γ-Al_2O_3. These tetrahedral and octahedral units are stacked without long-range order with some excess free volume located between the units. The local order in the other oxides studied here most likely resembles that from the anhydrous oxide as indicated by the similar α'_O. Therefore, the deviating pseudoboehmite Auger parameters are likely caused by the fundamentally different local structure of pseudoboehmite as compared to the other oxides in this study. For this reason, the results of pseudoboehmite will in the following be considered separately from the other oxides.

Initial State Parameters. The shifts observed in the measured O 1s binding energies of the various oxides are fully dominated by initial state effects, because the practically constant O Auger parameter α'_O (Table 3) implies that the contribution of final state effects (ΔR^{ea}, Table 3 and eq 2) is negligible. The total Al 2p binding energy shift observed is 0.5 eV (Table 1), while the extra-atomic relaxation changes over 0.25 eV but in the opposite direction (Table 3 and eqs 1 and 2). This then implies that the shifts observed in the Al 2p core level binding energies will to some extent also be influenced by final state effects.

The initial state parameters β_{Al} and β_O for respectively Al and O have been determined by using the measured electron core level binding energies and Auger electron transition kinetic energies (cf. eq 3 and Table 1). In Figure 4, the measured electron core level binding energies are plotted versus initial state parameters. For both Al and O, the initial state parameter increases with increasing core level binding energies and a linear relationship is observed for both β_O vs O 1s and β_{Al} vs Al 2p.

The initial state parameters of Al and O are composed of a contribution due to the charge q and Madelung potential, cf. eq 3. For the O anion, a direct evaluation can be made of the charge q present by considering the E_k(O $KL_{23}L_{23}$) − E_k(O KL_1L_{23}) peak separation.[28] This peak separation increases linearly with the O 1s core level binding energy for the studied oxides, see Figure 5. Thus, the O 1s binding energies are directly related to the surface-averaged charge q present on the anions. According to the work of Ascarelli et al.,[28] the peak separation range E_k(O $KL_{23}L_{23}$) − E_k(O KL_1L_{23}) of 19.7−21.0 eV (see Figure 5) corresponds to a surface-averaged charge q on the

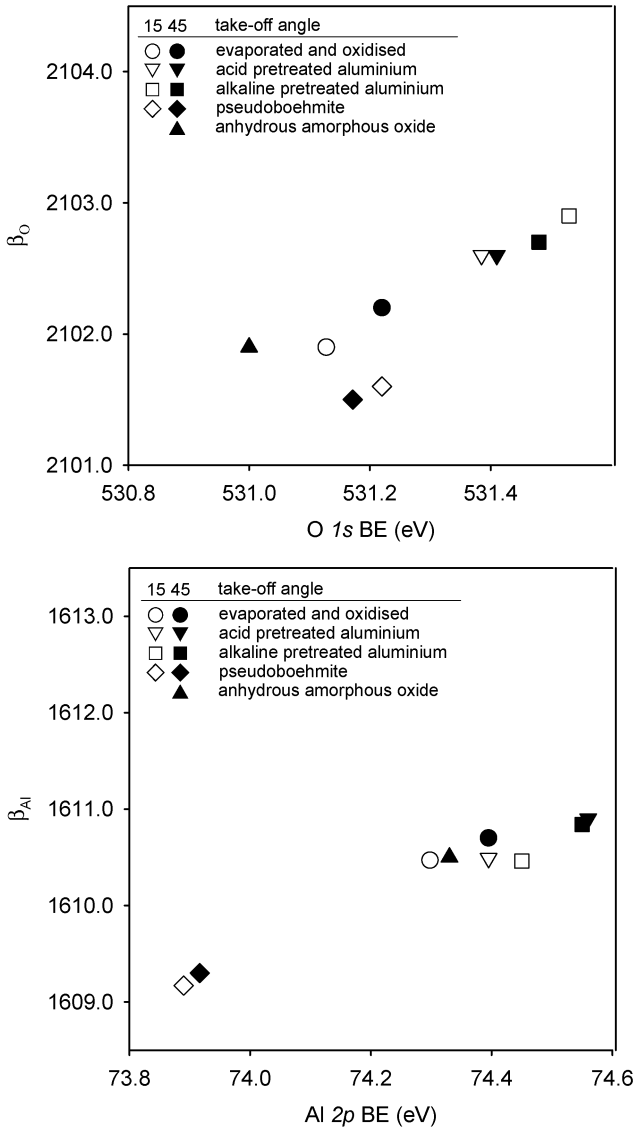

Figure 4. The initial state parameters versus their corresponding core level binding energies for oxygen (top) and aluminum (bottom) for the various aluminum oxides.

anions between about −1.2e for the alkaline-pretreated to about −1.7e for the anhydrous amorphous aluminum oxide.

In this context, it is noted that the binding energy shifts are not due to changes in Fermi level, as then a change in binding energy would not be reflected in a change in E_k(O $KL_{23}L_{23}$) − E_k(O KL_1L_{23}) peak separation and thereby in q. Moreover, the E(Al 2p − O 1s) peak separations, often used to separate Fermi-level shifts from chemical shifts,[32,33] does not show a constant value for the studied oxides, see Table 2. The pseudoboehmite oxide, being structurally different, shows deviating behavior from the other oxides. It has a much lower α'_{Al} and therefore a lower extra-atomic relaxation contribution to the O 1s binding energy, cf. eq 2. Also the initial state parameter β_O of the pseudoboehmite oxide is significantly lower than those of the other types of oxides, see Figure 4. However, the E_k(O $KL_{23}L_{23}$) − E_k(O KL_1L_{23}) versus O 1s binding energy values of all oxides, including pseudoboehmite, fall on a straight line, see Figure 5. Thus, the O 1s binding energy also for pseudoboehmite represents the charge q on the oxygen-containing anions (see above). Then, as compared to the other oxides (according to eq 1), the lower extra-atomic relaxation contribution must be compensated for by a lower Madelung potential contribution ΔV_M to the O 1s binding energy for pseudoboehmite.

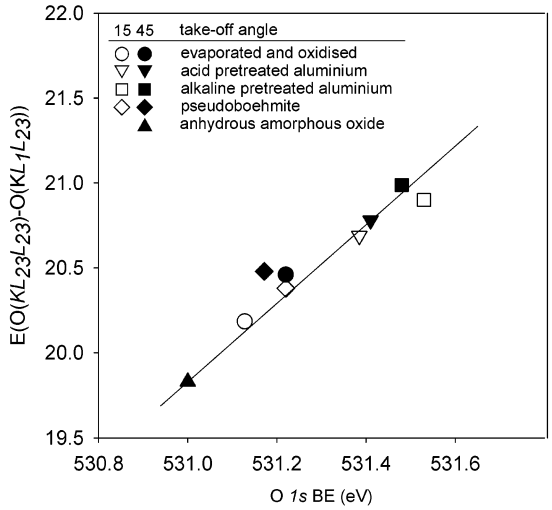

Figure 5. The distance between the O $KL_{23}L_{23}$ and the O KL_1L_{23} lines versus the O 1s core level binding energy for various aluminum oxide layers.

VI. Discussion

An evaluation of the measured core level binding energies (O 1s and Al 2p) and Auger electron kinetic energies (O KLL and Al KLL) for various aluminum oxides in terms of their initial state (β_{Al} and β_O) and final state (α'_{Al} and α'_O) parameters was performed. This analysis showed that for the *structurally comparable oxides* as evidenced from the similar value of their Auger parameter, see Table 3, the O 1s core level binding shifts *directly* represent changes in the initial state chemistry of the system and do not suffer from final state effects, cf. Figure 3 and Table 3. Moreover, it was shown that the O 1s core level binding energy shifts directly represent changes of the surface-averaged charge q present on the O anions and do not suffer from changes of the Madelung potential. The minor Al 2p core level binding energy shifts also correspond with changes in the initial state chemistry, cf. Figure 4, but these binding energy shifts do have a contribution from final state effects, cf. Table 3. It has been demonstrated that the core level binding energy shifts are not due to differences in the Fermi level of these oxides.

The O 1s binding energy increases in the order anhydrous oxide < evaporated and oxidized < acid-pretreated < alkaline-pretreated aluminum, for both takeoff angles, see Table 2. This implies that the surface-averaged electronic charge on the anions increases in the same order. The observed increases in O 1s binding energy can, however, be attributed solely to the increase of the OH component to the O 1s peak, which is present at a 1.3−1.4 eV higher binding energy, see section IV and Table 3. The binding energies of the separate components do not vary significantly for the oxides, see Table 2. Further, there are no differences observed in binding energy of the resolved components for the surface region (15° takeoff angle) and for the more bulk region of the oxide layer (45° takeoff angle). This indicates the absence of a surface oxide with a different chemistry for the ambient-exposed oxides. The chemical behavior of the separate hydroxyls (when present, see Table 2) and also oxygens is thus constant among the oxides. Therefore, the OH's will all have the same Brönsted/Lewis acid−base properties and the O's all the same Lewis base properties for all these oxides.

The Al 2p binding energy increases in the order anhydrous oxide < evaporated and oxidized < acid-pretreated < alkaline-pretreated aluminum, see Table 1. The increase of the Al 2p binding energy is small as compared to the shift observed for the O 1s peak, see Table 1. It has been demonstrated that there is a significant contribution of changes in extra-atomic relaxation to Al 2p core level binding energy shifts. This implies that there are only minor changes in chemical behavior for the Al cations for these oxides. There are no clear differences observed in binding energy for the surface region and for the more bulk region of the oxide layer, which indicates the absence of surface oxide, having a different chemistry. Thus, the Al sites for the different oxides are expected to have very similar Lewis acid properties.

The pseudoboehmite oxide shows significantly lower binding energies for its constituents as compared to the other oxides studied, see Table 2. However, the shift in binding energy cannot be used to directly ascribe this to changes in its initial state chemistry, see Figure 4, as the pseudoboehmite oxide is structurally different from the other oxides as evidenced from the Auger parameters, see Table 3. As discussed above, this results in different contributions to the core level binding energy as compared to the other oxides, see Figure 4. This signifies that a *direct* comparison of binding energy shifts to compare acid−base properties is only possible for structurally similar oxides. The position of pseudoboehmite in the initial state plots, see Figure 4, and the $E_k(\mathrm{O\ KL_{23}L_{23}}) - E_k(\mathrm{O\ KL_1L_{23}})$ versus O 1s plot, Figure 5, indicates that this oxide has OH, O, and also Al sites on its surface that are considerably more basic as compared to the other studied oxides.

It can be concluded that the oxides have very similar acid−base properties of their O, OH, and Al sites, with only the pseudoboehmite oxide showing more basic sites. However, the different oxides do show differences with respect to the *number* of hydroxyls present on their surfaces, cf. Table 2. These hydroxyls are for most organic functional groups directly involved in the chemical bonding mechanism.[1,2] Thus, an increase in the amount of hydroxyls will lead to a larger number of sites being available for interactions with organic molecules.

VII. Conclusions

Structurally similar oxide layers are formed when producing oxide layers with an alkaline or acidic pretreatment and by oxidizing aluminum in a vacuum, despite the different preparation procedures. The oxides exhibit OH sites with the same Brönsted/Lewis acid−base properties, O sites with the same Lewis base properties, and Al sites with very similar Lewis acid properties. Moreover, the oxides do not show a different chemistry on their surfaces as compared to the interior of the layers. The oxides do, however, differ in the amounts of hydroxyls that are present on their surfaces. After boiling aluminum in water, a pseudoboehmite oxide is formed, which is structurally different from the other oxides. This oxide has more basic O, OH, and Al sites.

XPS analysis evidenced that the values of the O 1s binding energies for the structurally similar oxides directly reflect the initial state chemistry of the anions. The oxides show shifts in their O 1s binding energy, but these are entirely due to changes in the amounts of hydroxyls in the oxide layer. The structurally different pseudoboehmite oxide has a lower extra-atomic relaxation and Madelung potential contribution to the binding energies. The O 1s binding energy is directly related to the surface-averaged charge present on the O-anions. This charge varies between about −1.2e for the oxide formed after an alkaline pretreatment to about −1.7e for the anhydrous amorphous aluminum oxide. A correlation between the Al 2p core level binding energy shift and the changes of the initial state chemistry of the oxides exists, but this Al 2p binding energy shift is also partially caused by changes in extra-atomic relaxation.

Acknowledgment. This research was carried out under project No. ME6.97026B in the framework of the Strategic Research program of The Netherlands Institute for Metals Research (NIMR) in The Netherlands. The authors gratefully acknowledge L.P.H. Jeurgens for providing the XPS software.

References and Notes

(1) Fowkes, F. M. *J. Adhes. Sci. Technol.* **1990**, *4*(8), 669−691.
(2) Fowkes, F. M. *Advances in Chemistry Series*; American Chemical Society: Washington, DC, 1964; No. 43, p 99.
(3) Barthes-Labrousse, M. G. *Vacuum* **2002**, *67*, 385−392.
(4) Davydov, A. A.; Rochester, C. H. *Infrared spectroscopy of adsorbed species on the surface of transition metal oxides*; Wiley: Chichester, UK, 1990.
(5) Barr, T. L. *Modern ESCA: The principles and practice of X-ray photoelectron spectroscopy*; CRC Press: Boca Raton, FL, 1994.
(6) Barr, T. L.; Brundle, C. R. *Phys. Rev. B* **1992**, *45*, 9199−9204.
(7) Barr, T. L. *J. Vac. Sci. Technol. A* **1991**, *9* (3), 1793−1805.
(8) Guittet, M. J.; Crocombette, J. P. *Phys. Rev. B* **2001**, *63*, 125117.
(9) Bosman, H. J. M.; Pijpers, A. P. *J. Catal.* **1996**, *161*, 551−559.
(10) Grunert, W.; Muhler, M. *J. Phys. Chem.* **1994**, *98*, 10920−10929.
(11) Stralin, A.; Hjertberg, T. *J. Appl. Polym. Sci.* **1993**, *49* (3), 511−520.
(12) Wernick, S.; Pinner, R.; Sheasby, P. G. *The surface treatment and finishing of aluminium and its alloys*, 5th ed.; ASM International: Teddington, OH, 1987; Vol. 1.
(13) Wefers, K.; Misra, C. *Oxides and hydroxides of aluminium*; Alcoa Technical Paper No. 19, 1987.
(14) Cocke, D. L. *Catal. Rev.* **1984**, *26* (2), 163−231.
(15) Siegbahn, K.; Nordling, C. *Nova Acta Regiae Soc. Sci. Ups.* **1967**, *4*, 20.
(16) Moretti, G. *J Electron Spectrosc.* **1998**, *95*, 95−144.
(17) Barr, T. L.; Seal, S. *J. Chem. Soc., Faraday Trans.* **1997**, *93* (1), 181−186.
(18) Bagus, P. S.; Illas, F. *J. Electron Spectrosc.* **1999**, *100* (1−3), 215−236.
(19) Pacchioni, G.; Bagus, P. S. *Phys. Rev. B* **1994**, *50*, 2576−2581.
(20) Vasquez, R. P. *J. Electron Spectrosc.* **1991**, *56*, 217−240.
(21) Wagner, C. D. *Anal. Chem.* **1972**, *44*, 967−973.
(22) Wagner, C. D. *J. Electron Spectrosc.* **1988**, *47*, 283−313.
(23) Wagner, C. D. *Faraday Discuss.* **1975**, *60*, 291−300.
(24) Moretti, G.; Filippone, F. *Surf. Interface Anal.* **2001**, *31*, 249−254.
(25) Moretti, G. *J. Electron Spectrosc.* **1992**, *58*, 105−118.
(26) Jeurgens, L. P. H.; Sloof, W. G. *J. Appl. Phys.* **2002**, *92* (3), 1649−1656.
(27) Snijders, P. C.; Jeurgens, L. P. H.; Sloof, W. G., to be submitted.
(28) Ascarelli, P.; Moreti, G. *Surf. Interface Anal.* **1985**, *7* (1), 8−12.
(29) Ealet, B.; Elyakhloufi, E. *Thin Solid Films* **1994**, *250*, 92−100.
(30) Weismann, R. *Solid State Commun.* **1979**, *31*, 347−349.
(31) Teterin, Y. A.; Ivanov, K. E. *J. Electron Spectrosc.* **1999**, *103*, 401−405.
(32) Mullins, W. M.; Averbach, B. L. *Surf. Sci.* **1988**, *206* (1−2), 29−40.
(33) Mullins, W. M.; Averbach, B. L. *Surf. Sci.* **1988**, *206* (1−2), 52−60.
(34) Jeurgens, L. P. H.; Sloof, W. G. *Thin Solid Films* **2002**, *418* (2), 89−101.
(35) Jeurgens, L. P. H.; Sloof, W. G. *Surf. Sci.* **2002**, *506* (3), 313−332.
(36) Alwitt, R. S. *Oxides and oxide films*; Dekker: New York, 1976; Vol. 4.
(37) American Society for Testing and Materials. *Surf. Interface Anal.* **1991**, *17*, 889.
(38) Seah, M. P.; Briggs, M. D. *Practical surface analysis*, 2nd ed.; Wiley: New York, 1990; Vol. 1.
(39) van den Brand, J.; Sloof, W. G. *Surf. Interface Anal.* **2004**, *36* (1), 81−88.
(40) Barrie, A. *Chem. Phys. Lett.* **1973**, *19* (1), 109−113.
(41) Eberhardt, W.; Kunz, C. *Surf. Sci.* **1978**, *75*, 709−720.
(42) Bianconi, A. *Phys. Rev. B* **1979**, *19* (6), 2837−2843.

(43) Jeurgens, L. P. H.; Sloof, W. G. *Appl. Surf. Sci*. **1999**, *144*−*145*, 11−15.
(44) Jeurgens, L. P. H.; Sloof, W. G. *Appl. Surf. Sci*. **2000**, *161*, 139−148.
(45) Barr, T. L. *Thin Solid Films* **1994**, *253*, 277−284.
(46) Barr, T. L. *J. Phys. Chem.* **1978**, *82* (16), 1801−1810.
(47) Olefjord, I. *Surf. Interface Anal.* **1990**, *15*, 681−692.
(48) Rotole, J. A.; Sherwoord, P. M. A. *J. Vac. Sci. Technol. A* **1999**, *17* (4), 1091−1096.
(49) Cordier, F.; Ollivier, E. *Surf. Interface Anal*. **1995**, *23*, 601−608.
(50) Alexander, M. R.; Thompson, G. E. *Surf. Interface Anal.* **2000**, *29*, 468−477.
(51) Frederick, B. G.; Apai, G. *Surf. Sci*. **1991**, *244*, 67−80.
(52) Fuggle, J. C. *J. Electron Spectrosc.* **1982**, *26*, 111−132.
(53) Wagner, C. D.; Zatko, D. A. *Anal. Chem* **1980**, *52* (9), 1445−1451.
(54) Rye, R. R.; Madey, T. E. *J. Chem. Phys.* **1978**, *68* (4), 1504−1512.
(55) Wagner, C. D. *J. Vac. Sci. Technol.* **1982**, *21* (4), 933−944.
(56) Remy, M. J.; Genet, G. J. *J. Phys. Chem*. **1992**, *96* (6), 2614−2617.
(57) Tessman, J. R.; Kahn, A. H. *Phys. Rev.* **1953**, *92* (4), 890−895.
(58) Scotto-Sheriff, S.; Darque-Ceretti, E. *J. Mater. Sci.* **1999**, *34*, 5081−5088.